Composite solid lipid nanoparticles with hydrogel core for delivering small hydrophilic molecules to the retina: an *in vitro* study using ARPE-19 and 661W cells.

Erico Himawan[a,1], Li Huang[b,1], Soumaya Belhadj[c], Raul Oswaldo Perez Garcia[d], François Paquet Durand[c], Nicolaas Schipper[d], Matej Buzgo[a], Valeria Marigo [b, *], Aiva Simaite[a, *]

[a]*InoCure s.r.o, Research and Development Department, Prague, Czech Republic*
[b] *Department of Life Sciences, University of Modena and Reggio Emilia, Italy*
[c]*Institute for Ophthalmic Research, Cell Death Mechanism Group, University of Tübingen, Germany*
[d]*Division Bioeconomy and Health -Chemical Processes and Pharmaceutical Development, Research Institute of Sweden, Sweden*

[1]These authors equally contributed to this work.
*Corresponding authors:
email addresses: aiva@inocure.cz, valeria.marigo@unimore.it

Count:
Abstract: 146 words; Manuscript: 4868 words; Tables: 2; Figures: 8; References: 38.

Abstract

Delivering small hydrophilic drug molecules to the retina is a challenging task in ophthalmology. A solid lipid nanoparticle (SLP) with a composite shell and hydrogel core as delivery system of a hydrophilic cargo to retinal cells has been developed in this work to meet the challenge. The composite shell formed by lipid and hydrophobic polyesters improves polydispersity while the hydrogel core enhances the encapsulation efficiency when compared to conventional SLP. *In vitro* studies tracking internalization and release of hydrophilic fluorescent dyes in retinal pigment epithelium and photoreceptor cell lines, showed a successful uptake and release of the hydrophilic cargo inside the cells. Validation of SLP encapsulation capability using a neuroprotective cGMP analogue resulted in a SLP size < 250 nm, negative surface charge > -20 mV, and encapsulation efficiency value of 60%. This formulation shows a potential to be applied as ocular drug delivery system and may open new perspectives for developing a treatment for retinal diseases.

Key words

661W; ARPE19; cGMP; drug delivery system; solid lipid nanoparticle.

Background

Retinal degeneration relates to different progressive diseases leading to vision loss, including diabetic retinopathy [1], age-related macular degeneration [2], and hereditary retinal degeneration [3]. Together, these diseases constitute an important health challenge that severely affect the quality-of-life of patients and has a significant socio-economic impact [4]. The cell types typically affected by these diseases are photoreceptors and retinal pigment epithelium (RPE) cells. While several different drugs have been proposed for treatment development, a key challenge is the delivery of an active pharmaceutical ingredient to the target cells within the retina and then maintain a large enough drug concentration over a prolonged period. This difficulty is exacerbated by the access-limiting blood retinal barrier. In this paper, we present a solid lipid nanoparticle (SLP) formulation with a composite shell and a hydrogel core that may be used as retinal drug delivery system (DDS).

In current clinical practice intravitreal injections are routinely used to administer treatments to the retina. This route allows DDS to bypass several ocular barriers like the corneal epithelium, the conjunctiva, and the sclera, while the vitreous and internal limiting membrane (ILM) will still need to be crossed. The vitreous has a gel-like network structure with a pore size expected to be in the range of 500 nm. Small drugs, proteins, and nanoparticles may diffuse through the vitreous [5,6]. A negatively charge surface and size below 500 nm are preferred qualities for DDS because these features may improve particle mobility [6,7]. When the drug requires intracellular targeting within the retina, barriers at the level of the plasma membrane will limit it's diffusion, especially for hydrophilic molecules [8]. DDS can help the delivery of the drug [9] and nanoparticles composed with material that enhances endocytosis, such as solid lipid nanoparticles (SLP), will likely improve the entrance of the active compound into the target cells [10–12].

Small hydrophilic cargo, like DNA [13] or cGMP analogue [14], are of major interest for treatment development. However, encapsulation of small hydrophilic molecules is challenging. Multiple DDS have been previously considered, such as liposomes [15] and polymeric particles [16]. However, these systems are characterized by low encapsulation efficiency, undesired leakage, or initial burst release [17]. For instance, when the water-in oil-in water ($W_1/O/W_2$) emulsion method is used to prepare lipid based particles such as liposomes, a small hydrophilic molecule can suffer low encapsulation efficiency due to leakage during preparation [18]. Other lipid based particles, like SLPs, are limited in space for uploading hydrophilic molecules [19] and compounds may be expelled following the polymorphic transition of the structure during storage [20]. To accommodate larger amounts of active molecules in the core of lipid based particles, and prevent their premature release, the addition of a thermo-responsive gel core [21] or of micelles [22,23] have been reported and shown to improve the encapsulation of hydrophilic cargo, such as proteins.

In this study we developed a new DDS formulated to hold small hydrophilic molecules by (*i*) incorporation of the compound inside a hydrogel, which forms the core of a SLP and (*ii*) combining a lipid and a hydrophobic polymer in the nanoparticle shell composition to improve its physicochemical characteristics. Rhodamine B (RhoB) was selected as a model drug/small hydrophilic cargo during development and the DDS encapsulation capability was validated using a phosphorothioate analogue of cGMP, named Rp-8-Br-PET-cGMPS (CN03), a compound that previously demonstrated to hold *in vivo* neuroprotective properties in the retina [24]. The resulting DDS was anionic with average particle size around 250 nm and high encapsulation efficiency (60%), characteristics important to overcome constrains for intravitreal route delivery (i.e., size, surface charge, encapsulation efficiency, and internalization ability). An *in vitro* test using photoreceptor and retinal pigment epithelium cell lines indicated that the DDS could help the process of small hydrophilic cargo internalization.

Methods

Materials

Poloxamer 407 (Sigma Aldrich), poloxamer 188 (Applichem), rhodamine B (RhoB; Sigma Aldrich), Rp-8-Br-PET-cGMPS, also known as CN03 (provided by Research Institute of Sweden), Glycerol tripalmitate (GTP; Alfa Aesar), soy-bean lecithin (LCT; VWR), stearic acid (SA; BASF), 50/50 DL-lactide/glycolide copolymer (PLGA; Corbion), poly-ε-caprolactone 14kDa (PCL; Sigma Aldrich), 8-aminonaphthalene-1,3,6-trisulfonic acid disodium salt (ANTS; Biotium), p-Xylene-Bis-Pyridinium Bromide (DPX; Biotium), dichloromethane (VWR), deionized water (VWR), ARPE-19 cell (ATCC), 661W cell (generously provided by Dr. Muayyad Al-Ubaidi, University of Oklahoma), Dulbecco's modified Eagle's medium and Ham's F12 nutrient mixture (DMEM/F12; Gibco), low glucose

(1mg/ml) Dulbecco's modified Eagle's medium (DMEM; Gibco), fetal bovine serum (FBS; Gibco), glutamine (Sigma Aldrich), penicillin-streptomycin (Sigma Aldrich), Accutase® solution (Sigma-Aldrich), paraformaldehyde (Sigma Aldrich), anti-Zonula occludens-1 (ZO-1) antibody (Invitrogen), goat anti-rabbit secondary antibody (Life technologies), 4',6-diamidino-2-phenylindole, dihydrochloride (DAPI; Sigma Aldrich), colorimetric methyl-thiazolyl diphenyl-tetrazolium bromide (Sigma Aldrich). All purchased materials were used as received.

Synthesis of solid lipid nanoparticles (SLPs)

SLPs consisting of a gel core and a composite shell have been developed using the double emulsion method with modifications [21–23]. Different formulations were prepared based on the composite shell composition (*i.e.*, presence and type of hydrophobic polymer) as well as its core composition (*i.e.*, presence of hydrogel core). RhoB was selected to track the particles inside the cells during the initial development. Both RhoB (479.02 g/mol) and the CN03 (562.3 g/mol) are highly hydrophilic and similar in size.

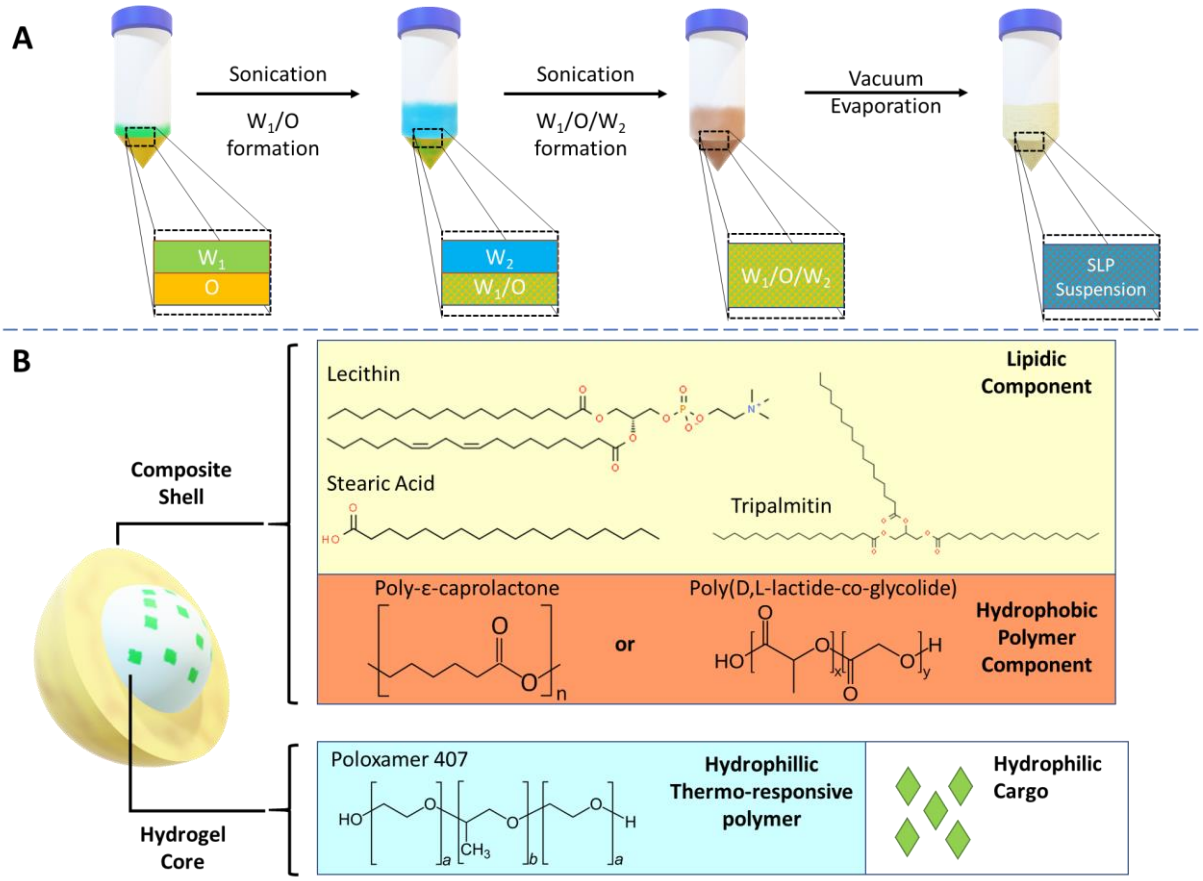

Figure 1. One pot synthesis of solid lipid nanoparticle consisting of a composite shell and a nanogel core. (**A**) formation of the SLPs suspension. (**B**) Composition of the composite SLPs.

The SLP formulation is illustrated in Figure 1. A stock solution for W_1-phase without gel core was prepared by dissolving RhoB in deionized water to reach 10 mg/ml concentration. For W_1-phase stock with gel core, poloxamer 407 was added to the RhoB solution to reach 40% w/v. To ensure complete dissolution, the poloxamer 407 solution was dissolved at 4°C for 48 h. The W_2-*phase* stock solution was prepared by dissolving poloxamer 188 in deionized water to reach 2% w/v concentration. The O-phase solution was prepared by dissolving GTP, LCT, SA, and PCL or PLGA in 1 ml of dichloromethane according to different formulation codes listed in Table 1. Finally, for the preparation of blank particle

and drug-loaded particle, deionized water and CN03 were used respectively in the W_1 phase instead of RhoB. Similarly, for release assays of the compound from SLPs inside the cell, ANTS and DPX were co-encapsulated in the W_1 phase instead of RhoB.

Table 1. Formulation code and component mass dissolved in O-phase for each formulation. DDS: drug delivery system; SLP: solid lipid nanoparticle; GTP: tripalmitin; LCT: soy-bean lecithin; SA: stearic acid; PCL: poly-ε-caprolactone; PLGA: 50/50 DL-lactide/glycolide.

DDS	GTP (mg)	LCT (mg)	SA (mg)	PCL (mg)	PLGA (mg)	Core
SLP.01	15	15	1	-	-	Aqueous
SLP.02	15	15	1	10	-	Aqueous
SLP.03	15	15	1	-	10	Aqueous
SLP.04	15	15	1	-	-	Hydrogel
SLP.05	15	15	1	10	-	Hydrogel
SLP.06	15	15	1	-	10	Hydrogel

The synthesis was performed by adding 200 µl of W_1-phase stock solution kept at 4-7°C, using an ice bath, to 1 ml of O-phase solution followed by sonication with the Q55 ultrasound probe from Qsonica (amplitude: 30% for 60 s without a pulse) to form the primary W_1/O emulsion. Then, 4.8 ml of W_2-phase solution was added into the primary emulsion and sonicated to form W_1/O/W_2 emulsion (amplitude: 40% for 10 s followed by 20 s at 20% amplitude without a pulse). The solution was further diluted with 10 ml of W_2-phase solution followed by sonication (amplitude: 20% for 30 s without a pulse). The organic solvent was then removed by vacuum evaporation at room temperature for 20 minutes to form the nanoparticles. The resulting colloidal solution was stirred for 4 h to ensure complete removal of dichloromethane.

For the analyses of compound release inside the cells, ANTS (25 µM) and DPX (90 µM) as a pair of tracer and quencher were co-encapsulated in the SLPs that were analyzed by a fluorescence quenching assay [25].

Physicochemical characterization

Dynamic laser scattering. The particle size distribution and hydrodynamic diameter were measured using NanoPhox DLS equipment from Sympatec, GmbH. Before the measurement, concentrated particle solution was diluted 5 times using 2% w/v poloxamer 188 solution. The analysis was performed using a non-negative least square (NNLS) algorithm integrated in Windox5 software from Sympatec, GmbH. Viscosity of the solution was calibrated and validated using the polystyrene bead standard. For each sample, measurement was repeated 6 times and each lasted 200 seconds.

Zeta potential. The zeta potential of the particle was measured by Zetasizer equipment from Malvern. Samples were diluted 5 times using 10 mM phosphate buffer, pH 7.4. For each sample, measurement was repeated 3 times.

Morphological analysis. SLP solution as described in table 1 was synthesized without hydrophilic cargo (i.e., blank particle) and analyzed using a transmission electron microscope (TEM). The colloidal nanoparticle solution was stained with 7% (w/v) phosphotungstic acid as a negative contrast. The morphological characterization of the particle was performed at an TEM acceleration voltage of 120 kV.

Encapsulation Efficiency. Encapsulation efficiency (EE) was measured using an indirect method in which the amount of unencapsulated cargo outside the particles was measured. Sample solutions were filtered using a 100 kDa microcentrifuge membrane filter (Sartorius) (3 x 5 minutes, @5000 RCF). The filtrate was collected, and the amount of cargo

was quantified using equation 1. As there might be some loss of W1-Phase in the pipette tips during synthesis, cargo loss was quantified to avoid encapsulation efficiency overestimation.

$$EE(\%) = (1 - \frac{cargo\ amount\ detected\ in\ filtrate}{Theoretical\ cargo\ amount - cargo\ loss\ in\ tips}) \times 100\% \quad (1)$$

RhoB and CN03 concentrations were quantified by measuring absorbance at 550 nm and at 254 nm using an UV-spectrophotometer (Biomolecular device) and high-pressure liquid chromatography (HPLC) system (Dionex Ultimate 3000), respectively. For HPLC, mobile phases A and B were 5 mM ammonium acetate buffer, and acetonitrile, respectively. 5µl of the sample were injected into the column (Waters® XBridge C18 XP column, 50 × 3 mm). The HPLC quantification was performed using Chromeleon software by calculating the peak area in the retention time around 3.1 minutes. Experiment was replicated 9 times for UV-spectroscopy and 3 times for HPLC.

***In Vitro* cell culture**

The human retinal pigment epithelial cell line (ARPE-19), was cultured in Dulbecco's modified Eagle's medium and Ham's F12 nutrient mixture (DMEM/F12) supplemented with 10% foetal bovine serum (FBS) and penicillin-streptomycin in a 5% CO_2 incubator at 37°C. The 661W cell line was cultured in low glucose (1 mg/ml) Dulbecco's modified Eagle's medium (DMEM) supplemented with 10% FBS, 2mM glutamine and penicillin-streptomycin in a 5% CO_2 incubator at 37°C. Approximately every three days cell cultures reached 70–80% confluence and the cells were passaged and sub-cultivated.

Fluorescence microscopic analysis and Immunofluorescence

Cells were seeded on glass coverslips in a 24-well plate at a density of 4×10^4 cells/well. 24 h later, cells were treated with RhoB encapsulated nanoparticles solution. As control, cells were treated with free RhoB solution at the same concentration (20 µM) of RhoB present in the nanoparticle solution. A blank was prepared by incubating the cells with nanoparticles containing no fluorophores. For compound release assays, 24 h after seeding, ARPE-19 cells were treated for 5 hours with medium containing 200 µg/ml blank SLP (blank), freely dissolved tracer or tracer/quencher pair (control), or 200 µg/ml SLP loaded with ANTS/DPX. Afterwards, the medium was replaced with non-treated fresh medium and the incubation was protracted for 24 h, 48 h or 72 h.

After incubation, cells were rinsed with phosphate buffer saline (PBS), fixed with 2% paraformaldehyde (PFA) for 10 minutes and nuclei were stained with 0.1 µg/ml 4′,6-diamidino-2-phenylindole (DAPI). For the immunofluorescence, after fixing with 2% PFA for 10 minutes, cells were incubated with anti-ZO1 (1:100) primary antibody overnight at 4°C. After washing three times with PBS, cells were incubated with the Alexa Fluor® 488 goat anti-rabbit secondary antibody (1:1000) and 0.1 µg/ml DAPI for 40 min at room temperature. Slides were mounted with Mowiol 4–88 and cells were observed using the Zeiss Axio Imager A2 fluorescence microscope.

Cell viability assay

Cell viability assay was performed by colorimetric methyl-thiazolyl diphenyl-tetrazolium bromide (MTT) assay. Cells were cultured in a 96-well plate at a density of 6,000 cells/well. After treatment with SLPs for different times, the medium was aspirated, and cells were incubated with 50 µl of 1 mg/ml MTT solution for 90 minutes at 37°C. The supernatant was removed, and the purple formazan crystals were dissolved in 100 µl isopropanol. The plate was shaken for 10 minutes and analysed at 570 nm using a microplate reader (Labsystems Multiskan MCC/340). The average absorbance was obtained from 3 biological

replicates.

Flow cytometry analysis

ARPE-19 and 661W cells were seeded on 12-well plates at a density of 1×10^5 cells/well. After treatment with control or SLPs, cells were detached with 500 µl Accutase® and collected by centrifugation at 300 G for 5 minutes at room temperature. The cells were washed three times with 500 µl PBS and collected by centrifugation at 300xg for 5 minutes at room temperature. The cell pellet was resuspended with 500 µl of PBS and RhoB fluorescence was immediately analyzed at the Attune® NxT Acoustic Focusing Cytometer. The channel voltage and gain were maintained constant throughout the whole analysis.

Statistical analysis.

Statistical analysis was performed using ANOVA, and $p < 0.05$ was considered significant.

Results

DDS development and analytical study.

With the purpose of developing a DDS to facilitate the uptake of hydrophilic molecules in retinal cells, we developed a procedure for SLPs with a size range of 200-250 nm (Table 2). The addition of hydrophobic polyesters such as PCL and PLGA notably improved particle polydispersity index to less than 0.4, and all nanoparticles produced were anionic as characterized by their zeta potential. The surface charge was similar for particles with and without hydrogel, *e.g.*, SLP.03 (-27 ± 2.3 mV) versus SLP.06 (-24 ± 1.5 mV). On the other hand, the presence of a hydrogel core improved the encapsulation efficiency, *e.g.*, SLP.02 (24 ± 0.8%) versus SLP.05 (47 ± 1.4%). Compared to SLP.01 (19 ± 1.7%), adding hydrophobic polyester to the shell formulation had no detectable effect on encapsulation efficiency, *i.e.*, all particles with an aqueous core had a RhoB encapsulation efficiency around 20%, while those with a hydrogel core could encapsulate above 40% of cargo regardless of the shell type. The DDS morphology observed using TEM confirmed that measured particles were below 500 nm as required for mobility in the vitreous (Figure 2).

Table 2. Summary of DDS physicochemical characteristic. SLP: solid lipid nanoparticle; PCL: poly-ε-caprolactone; PLGA: 50/50 DL-lactide/glycolide; PDI: polydispersity index; EE: Encapsulation Efficiency.

DDS	Shell	Core	Cargo	Size (nm)	PDI	Zeta Potential (mV)	EE (%)
SLP.01	Lipid	Aqueous	RhoB	218 ± 16.0	0.44 ± 0.02	-39 ± 2.1	19 ± 1.7
SLP.02	Lipid, PCL	Aqueous	RhoB	239 ± 3.2	0.30 ± 0.03	-15 ± 1.6	24 ± 0.8
SLP.03	Lipid, PLGA	Aqueous	RhoB	228 ± 0.9	0.34 ± 0.04	-27 ± 2.3	19 ± 2.8
SLP.04	Lipid	Hydrogel	RhoB	252 ± 19.3	0.44 ± 0.07	-41 ± 1.2	44 ± 3.0
SLP.05	Lipid, PCL	Hydrogel	RhoB	225 ± 2.3	0.22 ± 0.04	-13 ± 1.6	47 ± 1.4
SLP.06	Lipid, PLGA	Hydrogel	RhoB	237 ± 9.4	0.14 ± 0.05	-24 ± 1.5	45 ± 2.6
SLP.05	Lipid, PCL	Hydrogel	CNO3	257 ± 4.1	0.33 ± 0.03	-21 ± 3.9	60 ± 0.9
SLP.06	Lipid, PLGA	Hydrogel	CNO3	229 ± 3.6	0.38 ± 0.01	-25± 3.0	59 ± 1.0

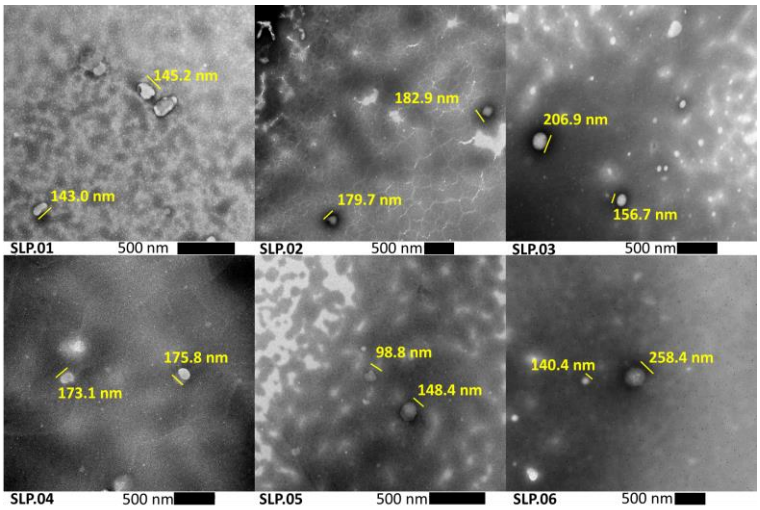

Figure 2. TEM analysis of particle morphology. Blank SLP particle without cargo was used for analysis.

Based on the analytical analysis of the different SLP generated, we chose to focus on SLP.05 and SLP.06 because they showed the best encapsulation efficiency together with a size below 500 nm and a negative surface charge, features necessary for intravitreal drug delivery to retina. Small size and negative charge should help the SLP to travel more freely within the vitreous [6,7].

In vitro cytotoxicity of nanoparticles

We then wanted to assess if these SLP could be taken up by retinal cells. In fact, active molecules should be internalized to reach their targets in RPE and photoreceptors, the cells primarily affected in retinal degeneration. For this study we chose two retinal cell types: ARPE-19, a spontaneously arising human RPE cell line with normal karyotype [26]; and 661W photoreceptor-like cells derived from a mouse retinal tumor generated in a transgenic mouse expressing SV40 large T-antigen under the control of *IRBP* (interphotoreceptor retinoid-binding protein) promoter [27].

We first wanted to assess whether and at which concentration the newly developed SLPs might be toxic to retinal cells, an important information for the prospective used in the clinic. To this purpose, a cell viability assay was performed on ARPE-19 and 661W cells. Cells were exposed to scaling concentrations of SLP.05 and SLP.06 nanoparticles for different time points.

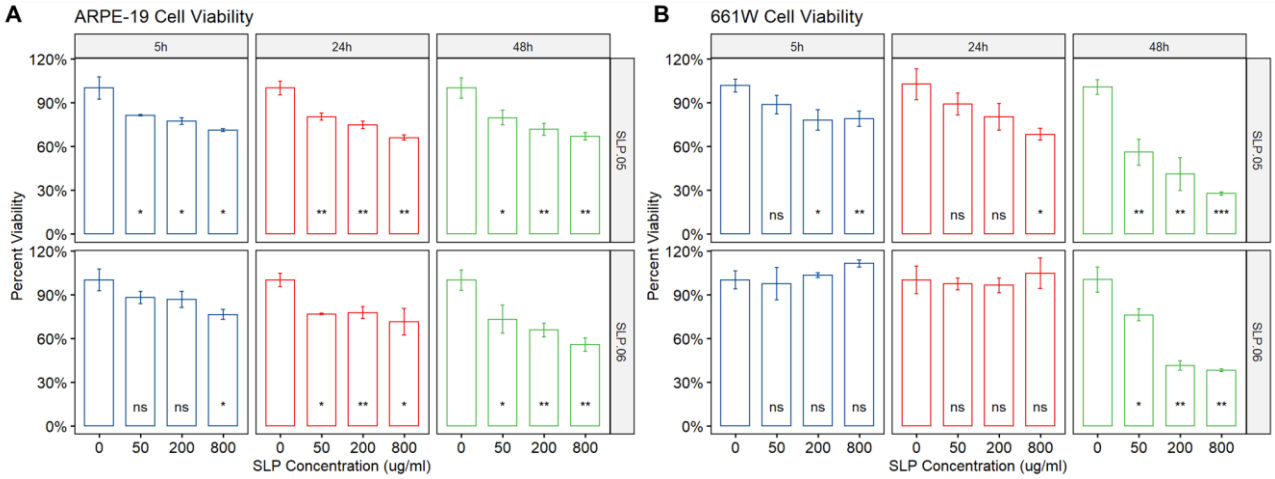

Figure 3. Cell viability study of ARPE-19 and 661W cells exposed to SLP.05 and SLP.06 at increasing concentrations (from 0 to 800 µg/ml) and for different duration time. Pairwise comparison against control at different time points for (**A**) ARPE-19 and (**B**) 661W cell line. *P<0.05,**P<0.01, ns: not significantly different, n = 3.

SLP.05 and SLP.06 displayed a dose-dependent toxicity on ARPE-19 cells (Figure 3A). A higher tolerance to SLPs was observed on 661W cells compared to ARPE-19, especially at 5 h and 24 h exposure time but toxicity was observed after prolonged exposure (Figure 3B). SLP.05 had a dose-dependent toxicity, which was maintained also at longer times of exposure and a drop in cell viability after 24 h of exposure was observed at all the tested concentrations. SLP.06, at concentrations up to 800 μg/ml, were quite well tolerated by 661W cells in the first 24 h of exposure.

Nanoparticle uptake by 661W and ARPE-19 cells

To define if the nanoparticles could be uptaken by the cells, SLP.05 and SLP.06 loaded with RhoB were applied to the 661W cells at increasing concentrations (Figure 4) for 5 h a time of exposure with limited toxicity. We observed an increasing fluorescence signal in correlation to the concentrations of SLP.05 (Figure 4A) and SLP.06 inside the cells (Figure 4B). RhoB loaded SLP.05 and SLP.06 were localized in the cytosol and excluded from the nuclei (blue) indicating internalization but not nuclear transfer.

When 200 μg/ml RhoB loaded SLP.05 and SLP.06 were applied to the ARPE-19 cells for 5 h, both types of SLPs were uptaken when compared to free RhoB or un-loaded SLPs (Figure 5). By labelling the cell boundaries with an antibody anti-zonula occludens-1 (ZO-1), we confirmed that RhoB loaded SLPs localized in the cytosol and did not enter the nucleus (Figure 6).

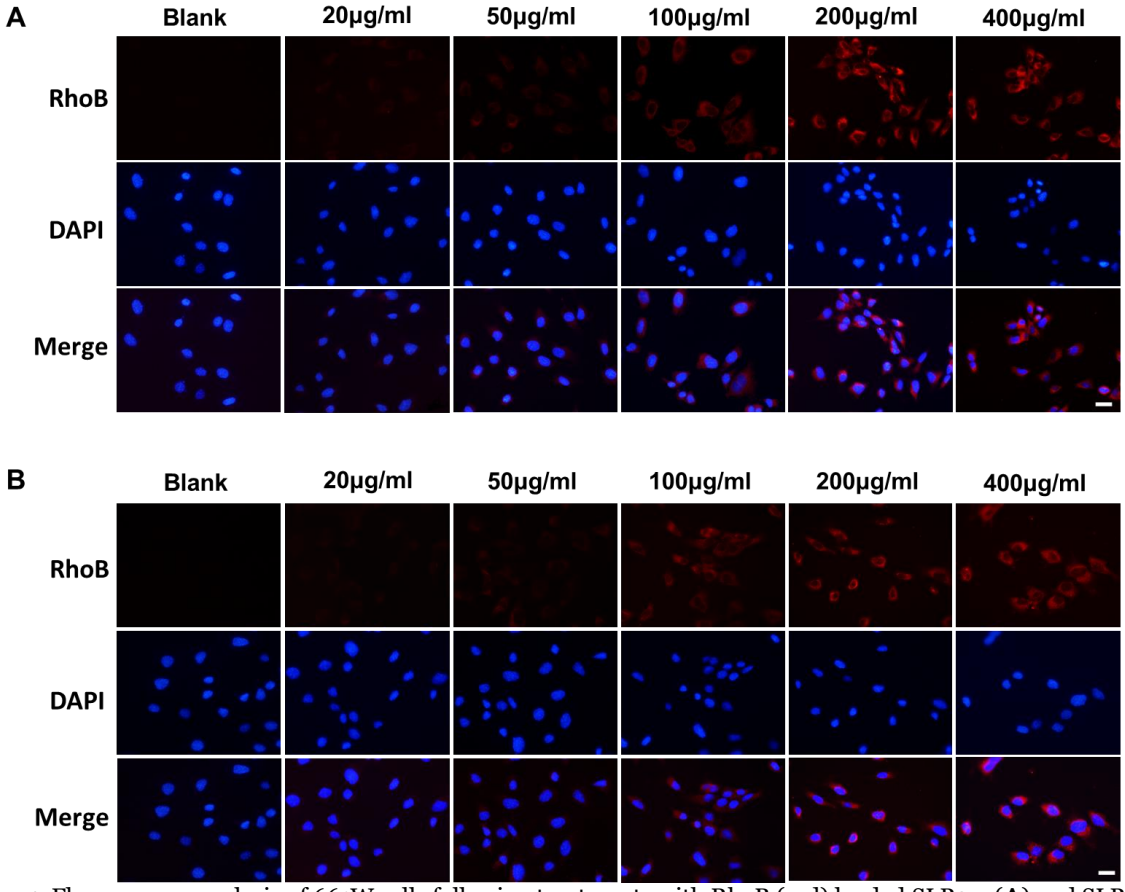

Figure 4. Fluorescence analysis of 661W cells following treatments with RhoB (red) loaded SLP0.5 (**A**) and SLP.06 (**B**) for 5 h at different concentrations. Blank: Cells treated with 200 μg/ml SLP.05 or SLP.06 without loading dye. Nuclei were stained with DAPI. RhoB concentration was kept constant at 20 μM for different SLP concentration. Scale bars: 20 μm.

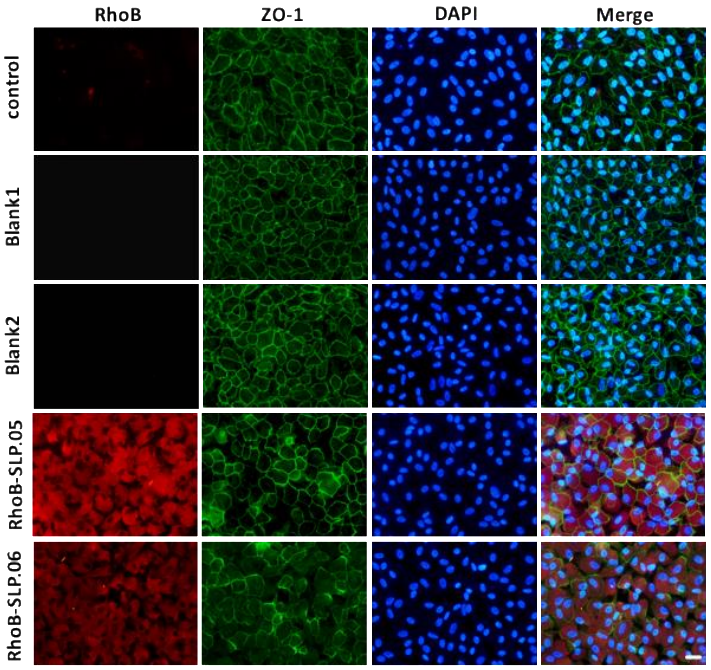

Figure 5. Immunofluorescent analyses of ARPE-19 cells following incubation for 5 h with 200 μg/ml RhoB (red) loaded SLP.05 and SLP.06. Control: cells cultured with freely dissolved 20 μM RhoB dye; Blank1: cells cultured with 200 μg/ml SLP.05 without dye; Blank2: cells cultured with 200 μg/ml SLP.06 without dye. RhoB concentration in RhoB loaded SLP is the same as in the control (20 μM). Tight junctions marking the boundaries of the cells were labelled using an antibody anti-ZO-1 (green). Nuclei were stained with DAPI. Scale bar: 20 μm.

To partially characterize the mechanism of SLP uptake, 661w cells were cultured with RhoB loaded SLP.05 and SLP.06 for 1 h at either 37°C or 4°C. Cells incubated at 4°C could not efficiently uptake SNPs, based on the absence of fluorescent signal, suggesting that energy-dependent endocytosis possibly mediated SLPs uptake in the cells [28].

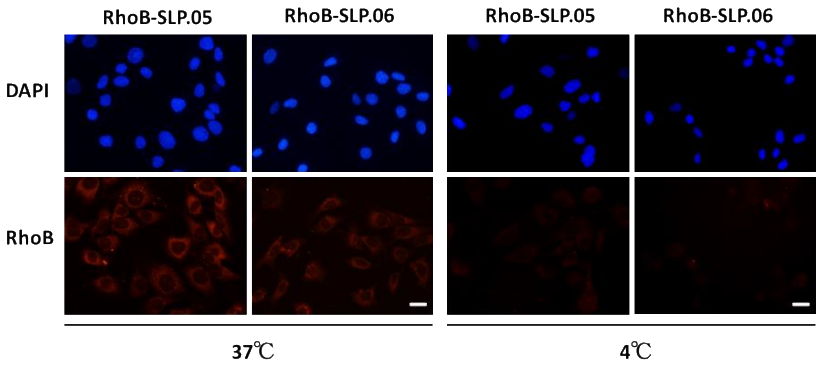

Figure 6. Fluorescence analysis of 661W cells following incubation for 1 h with 200 μg/ml RhoB loaded SLP.05 and SLP.06 at either 37°C or 4°C; RhoB concentration: 20 μM; Scale bars: 20 μm.

Quantification of nanoparticle internalization

A time course flow cytometry analysis was performed to quantify the uptake of SLP in the two retinal cell types. ARPE-19 and 661W cells were treated with 200 μg/ml of RhoB-loaded SLP.05 and SLP.06, and the fluorescence signal was quantified at different incubation times (1 h, 3 h, 5 h, and 24 h) by flow cytometry. Non-treated ARPE-19 and 661W cells were used as control. Gating was performed twice, with R1 gate to select the cell population and R2 gate to select RhoB positive cells based on blue laser (BL2-A) detector as shown in Figure 7A.

The graphical summary of the result is plotted over time in Figure 7B. The amount and intensity of fluorescent cells increased with prolonged incubation times. Notably, after 3 h

of incubation, around 48% of ARPE-19 cells had internalized SLP.05 particles and internalization increased to over 67% in 5 h. Uptake of SLP.06 was less efficient and required 24 h to reach about 16% (Figure 7B). 661W cells showed less internalization compared to ARPE-19 cells, with 13% RhoB on SLP.05 and 15% on SLP.06 after 5 h of exposure. In general, ARPE-19 cells displayed an increased SLP internalization with SLP.05 compared to 661W. On the other hand, SLP.06 showed similar SLP internalization levels between the two cell types.

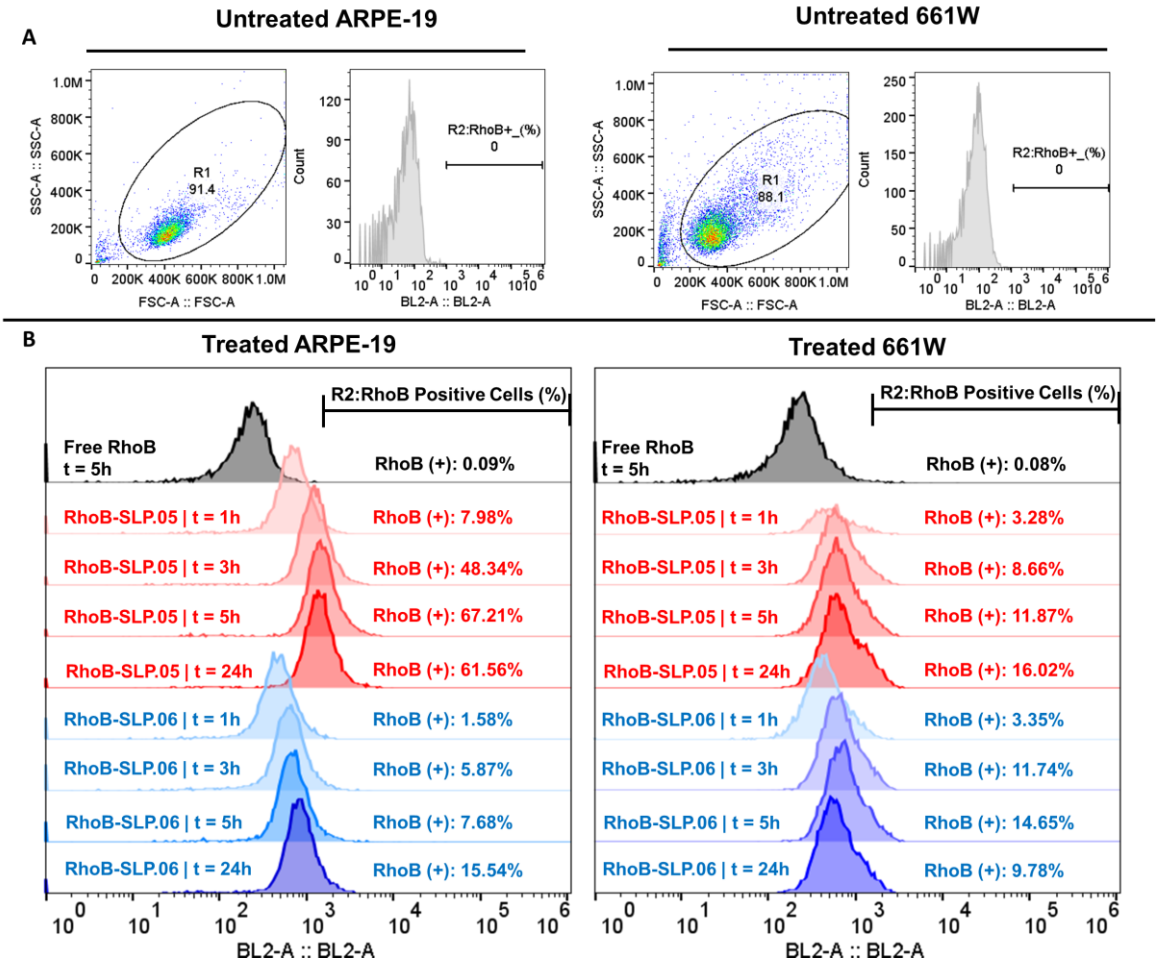

Figure 7. Flow cytometry analysis of fluorescence signal in ARPE-19 and 661W cells incubated with 200µg/ml RhoB loaded SLP.05 and SLP.06 at different time points. (**A**) Gating controls on each cell line for determining RhoB positive cells. (**B**) Histogram overlay of RhoB relative fluorescence intensity and RhoB positive cell percentage over different incubation time points. RhoB (+): percentage of cells with a fluorescent signal above the threshold defined in panel A. R1: Gating for selecting cells population; R2: Gating to select RhoB positive cells based on blue laser (BL2-A) detector; FSC-A: Forward scattering channel; SSC-A: Side scattering channel.

Release of the encapsulated cargo inside the cells

After demonstration of SLP internalization in retinal cells we wondered if the nanoparticle could release the encapsulated cargo after uptake. To address this issue, we co-encapsulated ANTS/DPX, a system previously published for fluorescence quenching assays to study vesicle leakage [29]. ANTS is a fluorescent dye that is quenched upon collision to the DPX molecule. ANTS fluorescence will increase upon breakage of SLP shell and release of cargo, because the quenching by DPX will diminish (i.e., increase of molecular distance leads to low collision probability) (Figure 8A). Based on this assay we could confirm that SLP could release the encapsulated compound after endocytosis. We observed that, overtime, a fluorescence signal could be detected in ARPE-19 cells exposed to SLP.05 and SLP.06 co-encapsulated with ANTS/DPX. The fluorescent signal was especially evident after

48 h. These data confirmed that the encapsulated cargo could be released from the nanoparticles once they entered cells.

Based on these promising results, as a proof of principle we evaluated if the newly developed SLPs could load a previously published compound, CNO3, demonstrated to be neuroprotective for the retina [24]. We were able to achieve about 60% encapsulation efficiency of CN03 while maintaining a negative charge and low size in SLP.05 and SLP.06 types of nanoparticles (Table 2).

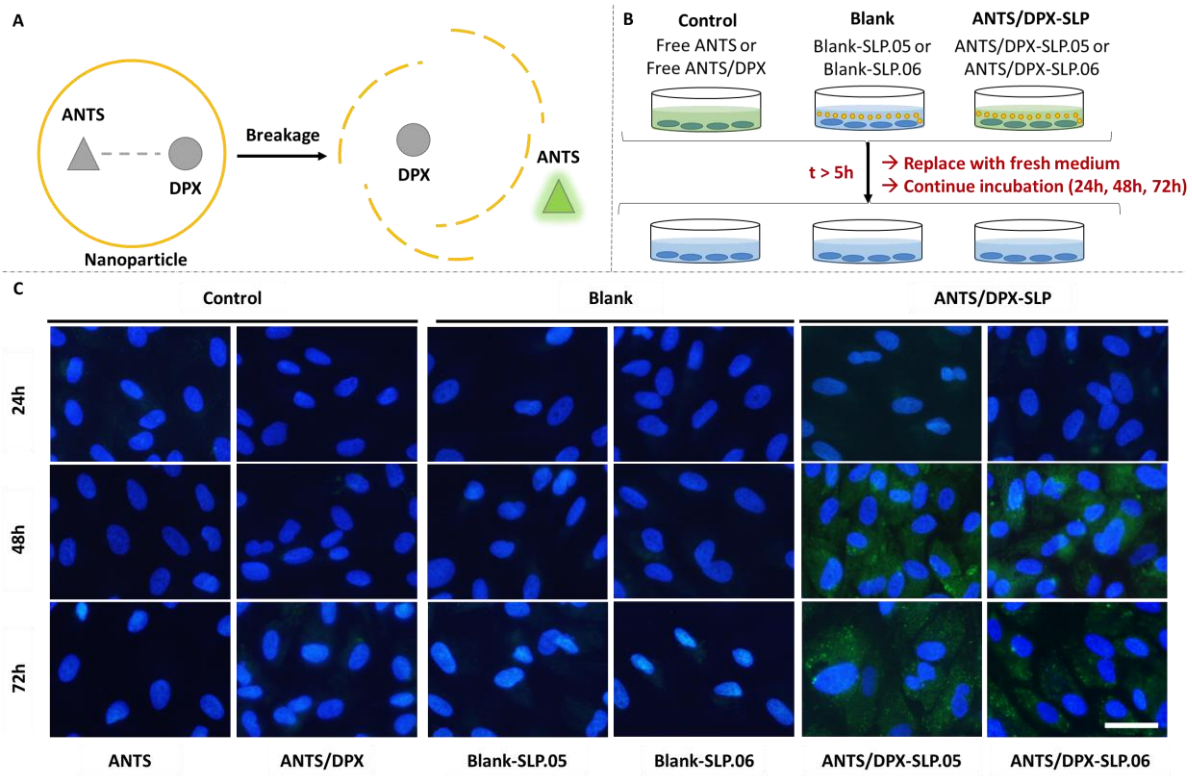

Figure 8. SLP breakage and its subsequent cargo release over time inside the cell. (**A**) Schematic representation of the concept of ANTS (fluorescence tracer) and DPX (quencher) usage. (**B**) Experimental setup: cells were incubated with control, blank and ANTS/DPX loaded SLPs for 5 h, then the medium was replaced with fresh medium and incubation continued for 24 h, 48 h and 72 h. (**C**) Fluorescence microscopy images taken at different incubation time points after 5 h incubation with ANTS/DPX loaded SLPs. Control: cells cultured with ANTS or ANTS/DPX; Blank: cells cultured with 200µg/ml SLP.05 or SLP.06 without any dye. ANTS/DPX-SLP: cells cultured with ANTS/DPX loaded SLP.05 or SLP.06. SLP concentration: 200 µg/ml; ANTS concentration: 25 µM; DPX concentration: 90 µM for. Scale bar: 20µm.

4. Discussion

The delivery of a drug to the neural retina is challenging due to the different barriers that need to be crossed and the physicochemical environment of the vitreous that needs to be considered. In this study we presented the formulation of nanoparticles which can enter retinal cells while having features that may facilitate the navigation across the vitreous. In the generation of the new SLP the key findings were: (*i*) the hydrogel core improved the encapsulation efficiency by up to 2-fold; (*ii*) the addition of hydrophobic polymer to the shell reduced particle polydispersity and improved the particle morphology. Overall, the SLPs generated here complied with the physicochemical property requirements for effective drug delivery to the neural retina by intravitreal route. Our results on encapsulation efficiencies suggested that the hydrogel core could improve the hydrophilic cargo retention during formulation. Most likely, the improved retention comes from the solidification of Poloxamer 407 emulsion droplets. This is in agreement with previously reported results showing that, thanks to the local increase in temperature during the sonication process, poloxamer 407 droplets formed a nanogel [21]. Meanwhile, the addition of polyester to the shell formulation reduced the strong negative charge of purely lipid SLPs shell (SLP.01; -39 mV) to different

extents depending on the hydrophobic polymer used. Particle shells containing PCL (SLP.02; -15 mV) had a higher zeta potential reduction compared to PLGA (SLP.03; -27 mV). Thus, the choice of polymeric components in the SLP composite shell may be used to tailor specific surface charge.

The size of the SLP was maintained in the range of 200-250 nm. There was an increase in surface charge when CN03 salts were used instead of RhoB in the SLP shell that contained PCL (SLP.05). Yet, this was not observed with the shell containing PLGA (SLP.06). Without CN03 salts, SLP.05 (-13 mV) had a lower charge than SLP.06 (-24 mV). This finding indicates that unencapsulated CN03 salts could preferably adsorb more on the less negatively charged surface. We also observed an increase in polydispersity when CN03 salts were used as cargo. Finally, there was about 15% increase in encapsulation efficiency of CN03 compared to RhoB. This may be due to the almost complete insolubility of CN03 salt in dichloromethane compared to RhoB. CN03, thus, hardly leaks out from W_1 phase during DDS preparation. In term of adaptability, we surmise that this system may also work for other small hydrophilic cargos with lower solubility in the organic solvent (*e.g.*, DNA).

Internalization studies in two retinal cell types demonstrated that: (*i*) the DDS formulation helped internalization of small hydrophilic compounds; (*ii*) the DDS shell component might be used to tailor the uptake rate in different cell types. We observed that ARPE-19 cells could better uptake SLP containing PCL in the shell (SLP.05). This might be due to the fact that SLP.05 is less negatively charged compared to SLP.06 and the uptake level is directly affected by physicochemical properties of SLPs, such as shape, size and surface charge [30]. In 661W cells, the uptake profile of SLP.06 nanoparticle was similar as for APRE-19 cells and limited to a low percentage of cells that internalized the nanoparticles. For SLP.05, less uptake was observed in 661W compared to ARPE-19. This difference may be attributed to the fact that uptake rates are also specific to each cell type [31]. It is not surprising that photoreceptor cells have a lower uptake rate compared to ARPE-19 cells, because RPE cells have a high rate of phagocytosis, in fact one of their functions is to phagocytose photoreceptor outer segments [32]. The reduced uptake at 4°C suggested that the SLPs mainly enter the cells via endocytosis, as the energy dependent endocytosis will be largely inhibited at this temperature [33–35]. Finally, we demonstrated that SLPs can release their cargo after being internalized by the cells. This result highlights that the newly developed DDS potential is appropriate for encapsulation of hydrophilic drugs and for their release into the target cells.

The *in vitro* cytotoxicity studies provided the insight that the two retinal cell lines were differently affected by our DDS. This is in agreement with previous studies reporting that distinctive cell physiology, proliferation rate, metabolic activity, membrane, and phagocytosis characteristics are responsible for the different sensitivity to external factors [36,37]. Physicochemical elements of nanoparticles can also affect the cytotoxicity of cells [37]. Specifically, SLP.05 and SLP.06, explaining distinct shell composition, were differently toxic to retinal cells. Our results suggest that the DDS shell type composition and concentration must be carefully tailored for the specific cell type that needs to be targeted.

While the relatively simple cell culture environment yielded interesting data, a full drug/DDS efficacy testing will likely require more complex test systems. More advanced *in vitro* tests using organotypic retinal explant cultures, in which the normal histotypic context of the retina is preserved [38], or *in vivo* injections will further characterize the suitability of the new SLPs for the delivery to the retina. Nevertheless, based on our formulation development and initial validation studies, this DDS appears to be suitable for intraocular administration of small hydrophilic compound for the treatment of retinal diseases.

Acknowledgements and funding information

We thank Prof Gareth R. Williams from University College London for his assistance in TEM images. We thank Dr. M. Montanari for technical support on flow cytometry. This

study was supported by grants from the European Union (transMed; H2020-MSCA-ITN-765441) and the Charlotte and Tistou Kerstan Foundation.

References

1 Lechner J, O'Leary OE, Stitt AW. The pathology associated with diabetic retinopathy. *Vision Res.* 139, 7–14 (2017).
2 Mitchell P, Liew G, Gopinath B, Wong TY. Age-related macular degeneration. *Lancet* 392(10153), 1147–1159 (2018).
3 Swaroop A, Sieving PA. The golden era of ocular disease gene discovery: Race to the finish. *Clin. Genet.* 84(2), 99–101 (2013).
4 Chakravarthy U, Biundo E, Saka RO, Fasser C, Bourne R, Little JA. The Economic Impact of Blindness in Europe. *Ophthalmic Epidemiol.* 24(4), 239–247 (2017).
5 Peeters L, Sanders NN, Braeckmans K *et al.* Vitreous: A Barrier to Nonviral Ocular Gene Therapy. *Investig. Opthalmology Vis. Sci.* 46(10), 3553 (2005).
6 Xu Q, Boylan NJ, Suk JS *et al.* Nanoparticle diffusion in, and microrheology of, the bovine vitreous ex vivo. *J. Control. Release* 167(1), 76–84 (2013).
7 Tavakoli S, Kari OK, Turunen T *et al.* Diffusion and Protein Corona Formation of Lipid-Based Nanoparticles in the Vitreous Humor: Profiling and Pharmacokinetic Considerations. *Mol. Pharm.* 18(2), 699–713 (2021).
8 del Amo EM, Rimpelä AK, Heikkinen E *et al.* Pharmacokinetic aspects of retinal drug delivery. *Prog. Retin. Eye Res.* 57, 134–185 (2017).
9 Himawan E, Ekström P, Buzgo M *et al.* Drug delivery to retinal photoreceptors. *Drug Discov. Today* 24(8), 1637–1643 (2019).
10 Apaolaza PS, del Pozo-Rodríguez A, Solinís MA *et al.* Structural recovery of the retina in a retinoschisin-deficient mouse after gene replacement therapy by solid lipid nanoparticles. *Biomaterials* 90, 40–49 (2016).
11 Bisht R, Mandal A, Jaiswal JK, Rupenthal ID. Nanocarrier mediated retinal drug delivery: overcoming ocular barriers to treat posterior eye diseases. *Wiley Interdiscip. Rev. Nanomedicine Nanobiotechnology* 10(2), 1–21 (2018).
12 Gorantla S, Rapalli VK, Waghule T *et al.* Nanocarriers for ocular drug delivery: Current status and translational opportunity. *RSC Adv.* 10(46), 27835–27855 (2020).
13 Gallego I, Villate-Beitia I, Martínez-Navarrete G *et al.* Non-viral vectors based on cationic niosomes and minicircle DNA technology enhance gene delivery efficiency for biomedical applications in retinal disorders. *Nanomedicine Nanotechnology, Biol. Med.* 17, 308–318 (2019).
14 Tolone A, Belhadj S, Rentsch A, Schwede F, Paquet-Durand F. The cGMP pathway and inherited photoreceptor degeneration: Targets, compounds, and biomarkers. *Genes (Basel).* 10(6), 1–16 (2019).
15 Kaiser JM, Imai H, Haakenson JK *et al.* Nanoliposomal minocycline for ocular drug delivery. *Nanomedicine Nanotechnology, Biol. Med.* 9(1), 130–140 (2013).
16 Chaharband F, Daftarian N, Kanavi MR *et al.* Trimethyl chitosan-hyaluronic acid nano-polyplexes for intravitreal VEGFR-2 siRNA delivery: Formulation and in vivo efficacy evaluation. *Nanomedicine Nanotechnology, Biol. Med.* 26, 102181 (2020).
17 Li Q, Li X, Zhao C. Strategies to Obtain Encapsulation and Controlled Release of Small Hydrophilic Molecules. *Front. Bioeng. Biotechnol.* 8(May), 1–6 (2020).
18 Zariwala MG, Bendre H, Markiv A *et al.* Hydrophobically modified chitosan nanoliposomes for intestinal drug delivery. *Int. J. Nanomedicine* 13, 5837–5848 (2018).
19 Khalkhali M, Mohammadinejad S, Khoeini F, Rostamizadeh K. Vesicle-like structure of lipid-based nanoparticles as drug delivery system revealed by molecular dynamics simulations. *Int. J. Pharm.* 559, 173–181 (2019).
20 Severino P, Pinho SC, Souto EB, Santana MHA. Polymorphism, crystallinity and hydrophilic–lipophilic balance of stearic acid and stearic acid–capric/caprylic triglyceride matrices for production of stable nanoparticles. *Colloids Surfaces B Biointerfaces* 86(1), 125–130 (2011).
21 Yang R, Gao RC, Cai CF *et al.* Preparation of gel-core-solid lipid nanoparticle: A novel way to

improve the encapsulation of protein and peptide. *Chem. Pharm. Bull.* 58(9), 1195–1202 (2010).
22 Chen C, Zhu X, Dou Y *et al.* Exendin-4 loaded nanoparticles with a lipid shell and aqueous core containing micelles for enhanced intestinal absorption. *J. Biomed. Nanotechnol.* 11(5), 865–876 (2015).
23 Xu Y, Zheng Y, Wu L, Zhu X, Zhang Z, Huang Y. Novel Solid Lipid Nanoparticle with Endosomal Escape Function for Oral Delivery of Insulin. *ACS Appl. Mater. Interfaces* 10(11), 9315–9324 (2018).
24 Vighi E, Trifunovic D, Veiga-Crespo P *et al.* Combination of cGMP analogue and drug delivery system provides functional protection in hereditary retinal degeneration. *Proc. Natl. Acad. Sci. U. S. A.* 115(13), E2997–E3006 (2018).
25 Martens TF, Remaut K, Demeester J, De Smedt SC, Braeckmans K. Intracellular delivery of nanomaterials: How to catch endosomal escape in the act. *Nano Today* 9(3), 344–364 (2014).
26 Dunn KC, Aotaki-Keen AE, Putkey FR, Hjelmeland LM. ARPE-19, A Human Retinal Pigment Epithelial Cell Line with Differentiated Properties. *Exp. Eye Res.* 62(2), 155–170 (1996).
27 Tan E, Ding X-Q, Saadi A, Agarwal N, Naash MI, Al-Ubaidi MR. Expression of Cone-Photoreceptor–Specific Antigens in a Cell Line Derived from Retinal Tumors in Transgenic Mice. *Investig. Opthalmology Vis. Sci.* 45(3), 764 (2004).
28 Firdessa R, Oelschlaeger TA, Moll H. Identification of multiple cellular uptake pathways of polystyrene nanoparticles and factors affecting the uptake: Relevance for drug delivery systems. *Eur. J. Cell Biol.* 93(8–9), 323–337 (2014).
29 Yang ST, Zaitseva E, Chernomordik L V., Melikov K. Cell-penetrating peptide induces leaky fusion of liposomes containing late endosome-specific anionic lipid. *Biophys. J.* 99(8), 2525–2533 (2010).
30 He C, Hu Y, Yin L, Tang C, Yin C. Effects of particle size and surface charge on cellular uptake and biodistribution of polymeric nanoparticles. *Biomaterials* 31(13), 3657–3666 (2010).
31 Kumari S, MG S, Mayor S. Endocytosis unplugged: multiple ways to enter the cell. *Cell Res.* 20(3), 256–275 (2010).
32 Bertolotti E, Neri A, Camparini M, Macaluso C, Marigo V. Stem cells as source for retinal pigment epithelium transplantation. *Prog. Retin. Eye Res.* 42, 130–144 (2014).
33 Behzadi S, Serpooshan V, Tao W *et al.* Cellular uptake of nanoparticles: journey inside the cell. *Chem. Soc. Rev.* 46(14), 4218–4244 (2017).
34 Palocci C, Valletta A, Chronopoulou L *et al.* Endocytic pathways involved in PLGA nanoparticle uptake by grapevine cells and role of cell wall and membrane in size selection. *Plant Cell Rep.* 36(12), 1917–1928 (2017).
35 Arana L, Bayón-Cordero L, Sarasola L, Berasategi M, Ruiz S, Alkorta I. Solid Lipid Nanoparticles Surface Modification Modulates Cell Internalization and Improves Chemotoxic Treatment in an Oral Carcinoma Cell Line. *Nanomaterials* 9(3), 464 (2019).
36 Kong B, Seog JH, Graham LM, Lee SB. Experimental considerations on the cytotoxicity of nanoparticles. *Nanomedicine* 6(5), 929–941 (2011).
37 Foroozandeh P, Aziz AA. Insight into Cellular Uptake and Intracellular Trafficking of Nanoparticles. *Nanoscale Res. Lett.* 13(1), 339 (2018).
38 Belhadj S, Tolone A, Christensen G, Das S, Chen Y, Paquet-Durand F. Long-Term, Serum-Free Cultivation of Organotypic Mouse Retina Explants with Intact Retinal Pigment Epithelium. *J. Vis. Exp.* (165) (2020).

May 21, 2021